Effect of Laser Surface Remelting on the Corrosion Resistance of 316L Orthodontic Brackets

Xiao-Yan ZHANG[1], Yong ZOU[2,] , Xiang-Long ZENG[3,*]*

[1] Department of Orthodontics, Beijing Stomatological Hospital, Capital Medical University, Beijing 100006，China
[2] Key Lab of Liquid Structure and Heredity of Materials, Ministry of Education, Shandong University, Jinan 250061, Shandong, China
[3] Department of Orthodontics, School & Hospital of Stomatology, Peking University，Beijing 100081, China
[*]E-mail: yzou@sdu.edu.cn or zengxl@yeah.net

To improve its corrosion resistance from artificial saliva, 316L orthodontic brackets were subjected to surface modification by laser remelting. The experimental results showed that the passive films of 316L orthodontic bracket in artificial saliva have n-type semiconducting properties. The improvement of 316L orthodontic bracket corrosion resistance was found to depend on the laser power. Laser surface remelting decreased the amount of δ second phase in the 316L orthodontic bracket. However, only the appropriate laser power was found to improve its corrosion resistance. Moreover, high laser powers were unable to increase its corrosion resistance. The improved corrosion resistance of 316L orthodontic bracket was attributed to the refinement of its grain sizes and homogenization of its surface elements by laser remelting.

1. INTRODUCTION

Austenitic stainless steels have the appropriate mechanical properties, such as a high ultimate tensile strength, and good corrosion resistance, that enable their use on a wide range of technological applications, including orthodontic treatments [1,2–4]. Type 316L stainless steel is the most commonly used material in orthodontic brackets. Orthodontic brackets are exposed to potentially damaging physical and chemical agents in oral environments, which could cause corrosion and affect the integrity of orthodontic brackets, such as the 316L orthodontic bracket [5,6]. Thus, orthodontic

brackets should be made of highly corrosion-resistant metals and/or metal alloys. The corrosion resistance of 316L orthodontic brackets have been studied by various authors at simulated physiological conditions [7–10]. Surface modifications have been reported to improve the corrosion resistance of austenitic stainless steel [11,13]. Among the various techniques used for surface strengthening, laser surface-engineering technology is an advanced surface-modification technology, in which metal surfaces are quickly melted and then rapidly solidified [14–16]. Laser surface modification is based on the use of laser as a heat source to modify the surface properties of components. Currently, it has been widely used in fabricating protective coatings to improve the wear- or corrosion-resistant properties of their components. In a previous study, the passive film theory on the corrosion resistance of stainless steel has been widely accepted[17.18]. However, the properties of the passive film on austenitic stainless steel in artificial saliva remain unknown. Moreover, studies on the effect of laser surface treatment on the passive film and corrosion resistance of stainless steel are limited.

This study aimed to determine the effect of laser surface remelting on the corrosion resistance of austenitic stainless steels in artificial saliva. The properties of the passive film, such as its semiconducting properties and donor densities, were studied via electrochemical techniques. The relationships between the laser processing parameters and the corrosion resistance of the modified surface layer were also analyzed.

2. EXPERIMENTAL PROCEDURE

AISI 316L austenitic stainless steel was used as the raw material for the orthodontic brackets. The AISI 316L austenitic stainless steels were chemically composed of the following (in wt.%): C 0.022, Si 0.65, Mn 1.94, S 0.03, P 0.041, Cr 18.36, Ni 11.52, Mo 2.29, and Fe bal. Laser surface remelting was conducted using a Rofin FL-010 fiber laser with a 2 mm defocused laser beam. The laser has approximately 300 W to 500 W output power and approximately 2 mm/s laser scan speed. A side jet of argon with 15 L/min gas flux was used to prevent sample oxidation. A multitrack with 30% overlap ratio was produced to create the modified layer. The base metal and samples were remelted with the laser at 300, 400, and 500 W and were denoted as No. 1, No. 2, No. 3, and No. 4, respectively. The artificial saliva used was composed of 0.4 g/L NaCl, 0.4 g/L KCl, 0.795 g/L $CaCl_2 \cdot 2H_2O$, 0.780 g/L $NaH_2PO_4 \cdot 2H_2O$, 0.005 g/L $Na_2S \cdot 9H_2O$, 1 g/L urea, and 1 L distilled water. The tested media had an approximate pH of 6.8. A D/Max-2500PC x-ray diffractometer with Cu–Kα radiation operated at 60 kV and 40 mA was used to analyze the phase structures of the samples. Microhardness of these samples was measured by using a Shimadzu HMV-2000 type micro Vickers, and an average value of hardness was taken from three measurements

A three-electrode electrochemical-cell system was used in this study, with the sample material as the working electrode, platinum plate as the counter electrode, and +0.241 V_{SHE} saturated calomel electrode (SCE) as the reference electrode. Potentiodynamic polarization scans were conducted at 1 mV/s sweep rate and −1.2 V (vs. SCE) to 1.2 V (vs. SCE) scan range. The electrochemical impedance spectroscopy (EIS) measurements were carried out with 10 mV amplitude and 0.01 Hz to 10 kHz

frequencies after immersion a certain time. The Mott–Schottky plots were obtained by performing a potential scan from −0.6 V (vs. SCE) to 0.9 V (vs. SCE) at a 1000 Hz fixed frequency. Each test was repeated at least thrice to ensure the reproducibility of the results.

Mott–Schottky relationship expresses the potential dependence of the space–charge layer capacitance (C_{sc}) as follows:

$$\frac{1}{C_{sc}^2} = \frac{2}{e\varepsilon\varepsilon_0 N_D A^2}(E - \phi_{fb} - \frac{kT}{e}) \qquad \text{for n-type semiconductor} \qquad (1)$$

$$\frac{1}{C_{sc}^2} = \frac{2}{e\varepsilon\varepsilon_0 N_A A^2}(E - \phi_{fb} - \frac{kT}{e}) \qquad \text{for p-type semiconductor} \qquad (2)$$

N_D and N_A can be determined from the slope of the linear relationship (K) in the Mott–Schottky plots as:

$$K = \frac{2}{e\varepsilon\varepsilon_0 N_D A^2} \qquad \text{for n-type semiconductor} \qquad (3)$$

$$K = \frac{2}{e\varepsilon\varepsilon_0 N_A A^2} \qquad \text{for p-type semiconductor} \qquad (4)$$

where e is the electron charge (1.60×10^{-19} C), ε is the dielectric constant of Fe oxide (15.6) [18], ε_0 is the vacuum permittivity constant (8.85×10^{-14} F·cm^{-1}), N_D and N_A are the donor and acceptor density values, respectively, E is the applied potential (the horizontal ordinate in the Mott–Schottky plots), k is the Boltzmann constant (1.38×10^{-23} J·K^{-1}), T is the absolute temperature (t + 273.15 K), and A is the area of the specimen, which was obtained in 1 cm^2 in the experiments.
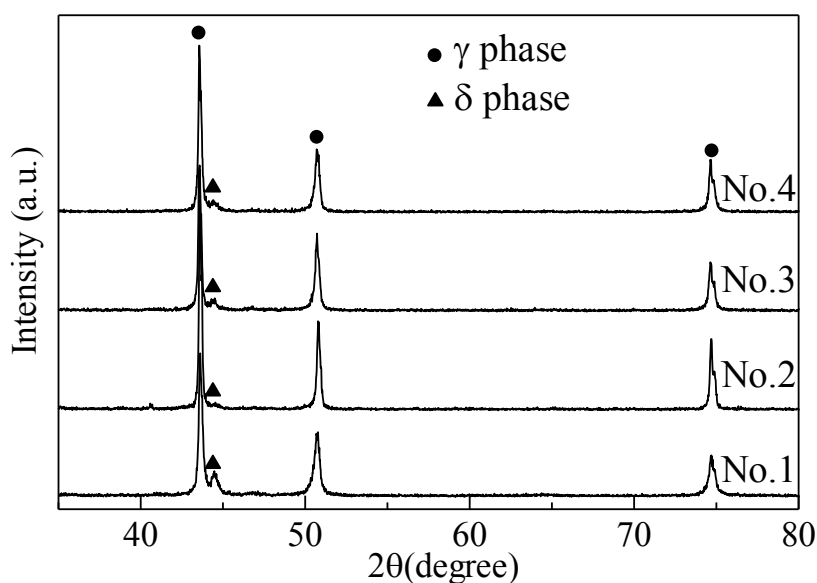
3. RESULTS AND DISCUSSION

Figure 1. The X-ray diffraction pattern of the base metal sample and laser remelting samples.

Figure 1 shows the X-ray diffraction pattern of the 316L orthodontic bracket before and after laser remelting with different laser powers. As indicated in Fig. 1, the base metal (No. 1) consisted of γ and δ phases, with the δ phase estimated at about 11% based on the X-ray diffraction pattern. After laser surface remelting, the amount of δ phase decreased to about 1%, which indicated that laser surface remelting changed the phase structure of austenitic stainless steel. In addition, the full width at half maximum of the base metal and the samples subjected to 300, 400, and 500 W laser surface remelting were 0.272, 0.172, 0.192, and 0.218, respectively.
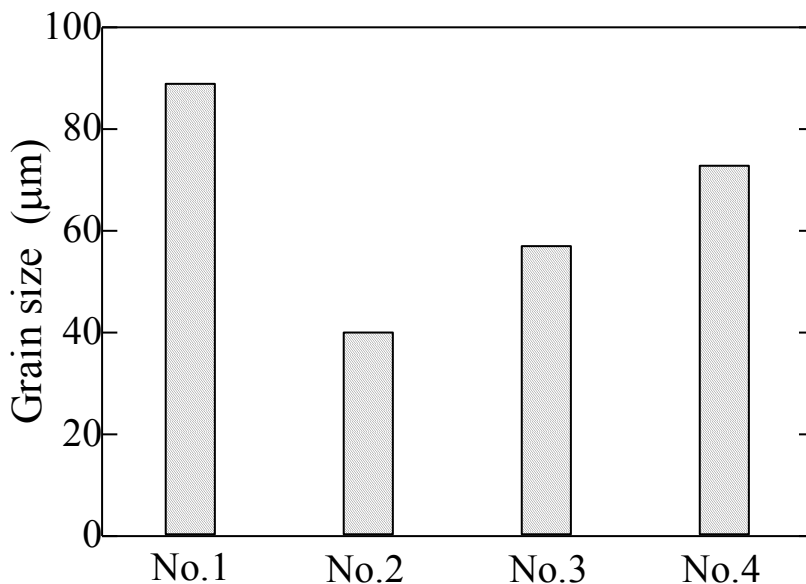

Figure 2. The grain size of the base metal sample and laser remelting samples.
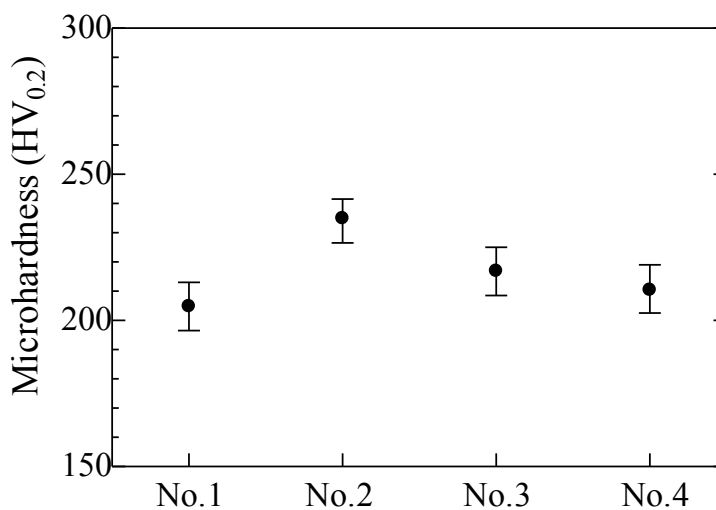

Figure 3. The microhardness of the base metal sample and laser remelting samples.

Figure 2 gives the grain size of the samples, which are calculated from the X-ray data. These results suggested that laser surface remelting refined the grain sizes, which were found to increase with increasing laser power. The variation of microhardness of these samples is indicated in Fig.3, which is corresponded to the variation of grain size.
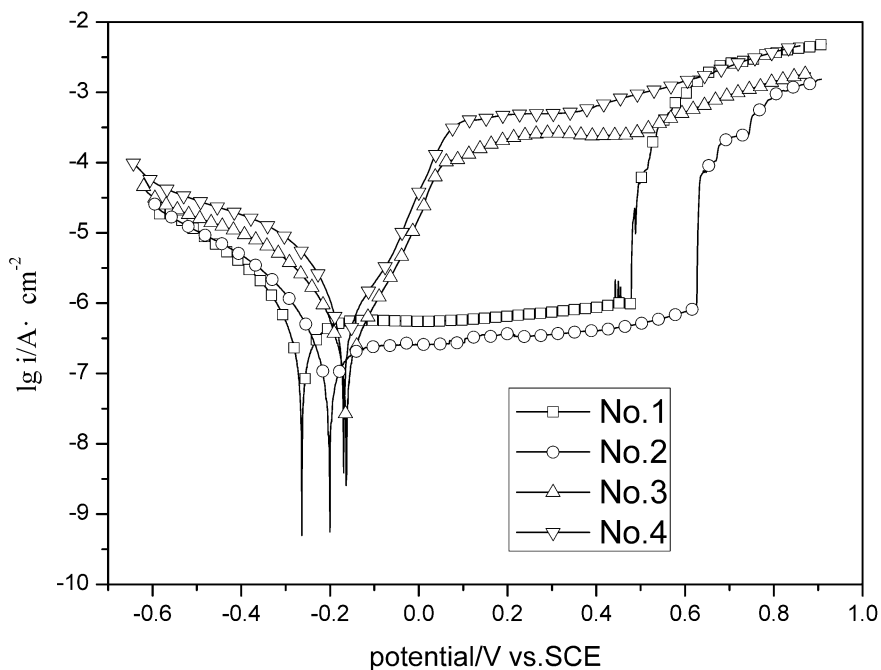

Figure 4. The potentiodynamic polarization curves of the samples in artificial saliva.

Figure 4 shows the respective potentiodynamic polarization curves of the samples in artificial saliva. The corrosion potential (E_{corr}) and corrosion current density (i_{corr}) were calculated from the potentiodynamic polarization curves via Tafel extrapolation method; the results are listed in Table 1. The corrosion potential was found to shift at higher potentials with increasing laser melting power. However, No.1 and No. 2 samples were also found to demonstrate evident passive zones and lower corrosion currents. In particular, No. 2 sample, which was subjected to 300 W laser remelting power, showed the lowest corrosion current and the best corrosion resistance. However, No. 3 and No. 4 samples, which were treated with higher laser powers, exhibited narrower passive zones and higher corrosion currents. These results revealed that higher laser powers decreased corrosion resistance.

Table 1. Corrosion parameters obtained from the polarization curves of samples

samples	Tafel Slope (b_c), mV/decade	I_{corr} (mAcm^{-2})	E_{corr}(V)	V(mm/a)
No.1	91.769	0.30836	-0.26346	0.003627
No.2	84.116	0.2934	-0.16921	0.003451
No.3	116.05	0.32003	-0.1632	0.0037642
No.4	141.25	0.32813	-0.20068	0.0038596

Electrochemical impedance spectroscopy was measured to study the effects of laser remelting on the corrosion behavior of stainless steel. The EIS measurements were conducted at open circuit potential, and the results are shown in Fig. 5. As shown in Fig. 5(a), the Nyquist plots contained two capactive loops. The capacitive reactance loop in high and low frequency regions corresponded to the electric double layer and corrosion process, respectively.
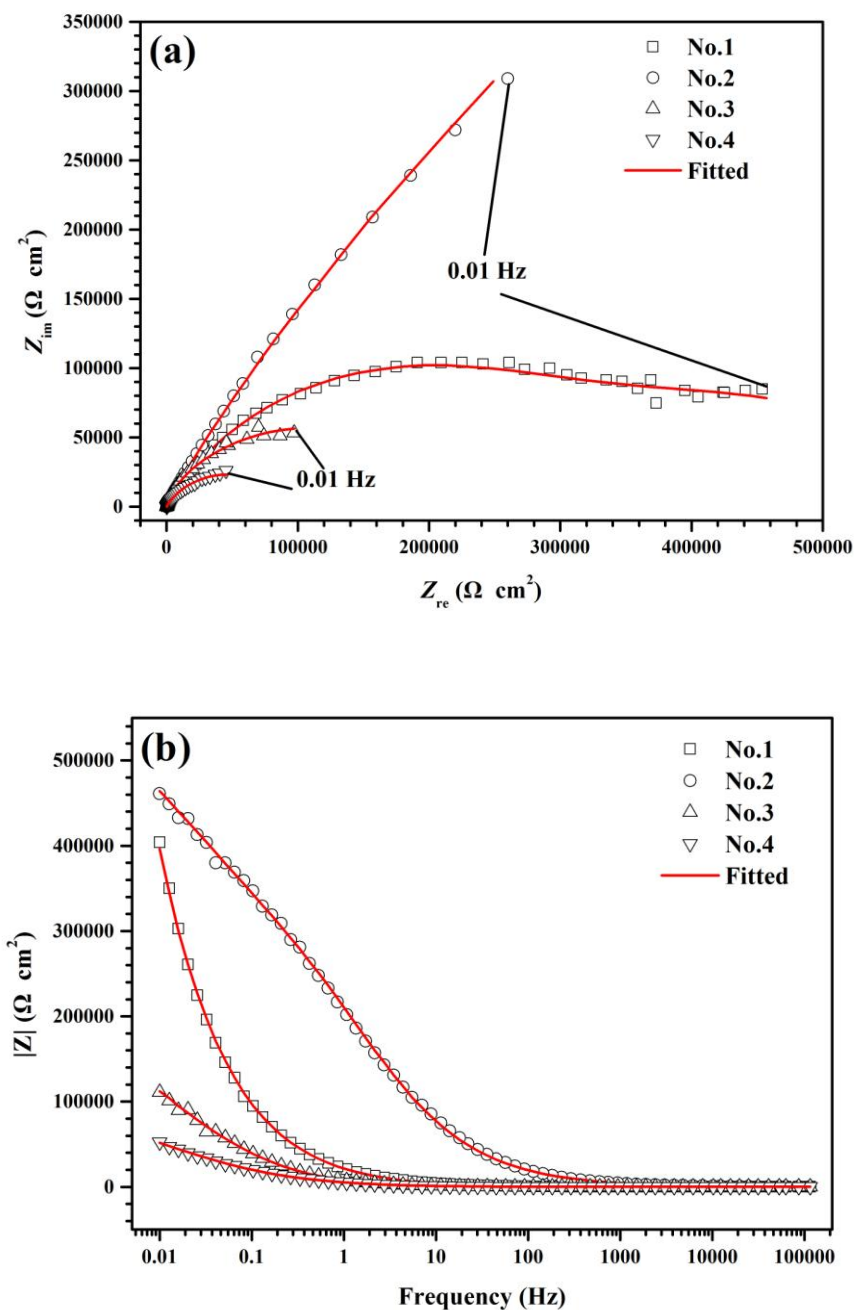

Figure 5. Experimental and fitted EIS results of as-received and laser remelted samples; (a) Nyquist plots and (b) Bode plots
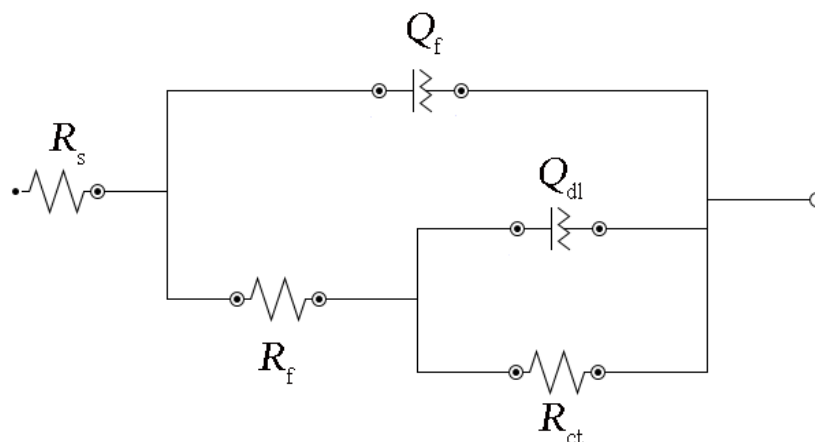
Figure 6. Equivalent circuit of $R_s(Q_f(R_f(Q_{dl}R_{ct})))$

The equivalent circuit of Rs{Qf[Rf(QdlRct)]}, as shown in Fig. 6, was used to simulate the EIS results. As shown in Fig. 6, the good agreement was obtained. In the circuit, Rs is the solution resistance, Qdl and Qf are the constant–phase element (CPE) of electrical double-layer and corrosion product film, respectively, and Rf and Rct are the corrosion product film and charge transfer resistance, respectively. CPE was used as the non-ideal capacitance of the electrical double-layer and the corrosion product film to account for their heterogeneity and toughness, as follows: $Z_{CPE} = [Q(jw)^n]^{-1}$, where $j = \sqrt{-1}$, n is the CPE exponent, and w is the angular speed. ZSimpWin software was used to analyze the values. The fitting results for every parameter are shown in Table 2, and change regulars of Rct and Rf are shown in Fig. 7.

Table 2. Fitted results of EIS

		No.1	No.2	No.3	No.4
	R_s (Ω cm^2)	80.64	134.8	150.3	168.7
Q_f	Y_f (W^{-1} cm^2 S^n)	7.533e-7	9.353e-6	2.68e-5	1.672e-6
	n_f	0.6491	1	0.825	1
	R_f (Ω cm^2)	3.193e5	699.1	6.757e4	6.395e5
Q_{dl}	Y_{dl} (W^{-1} cm^2 S^n)	1.12e-5	5.141e-5	3.846e-5	1.234e-5
	n_{sl}	0.4555	0.5679	0.5666	0.6119
	R_{ct} (Ω cm^2)	3.203e5	9.237e4	1.501e5	3.445e6

It can be seen that the Rct and Rf of the laser-remelted sample when the power is 300 w is obviously bigger than those of the as-received sample. In addition, the Rct and Rf decrease as the power increase. The Rct and Rf of the laser-remelted samples when the power is 400 w and 500 w are worse than those of the as-received sample. It is indicated that the corrosion resistance is better when the power is 300 w. The EIS results are in accordance with the polarization curves results.
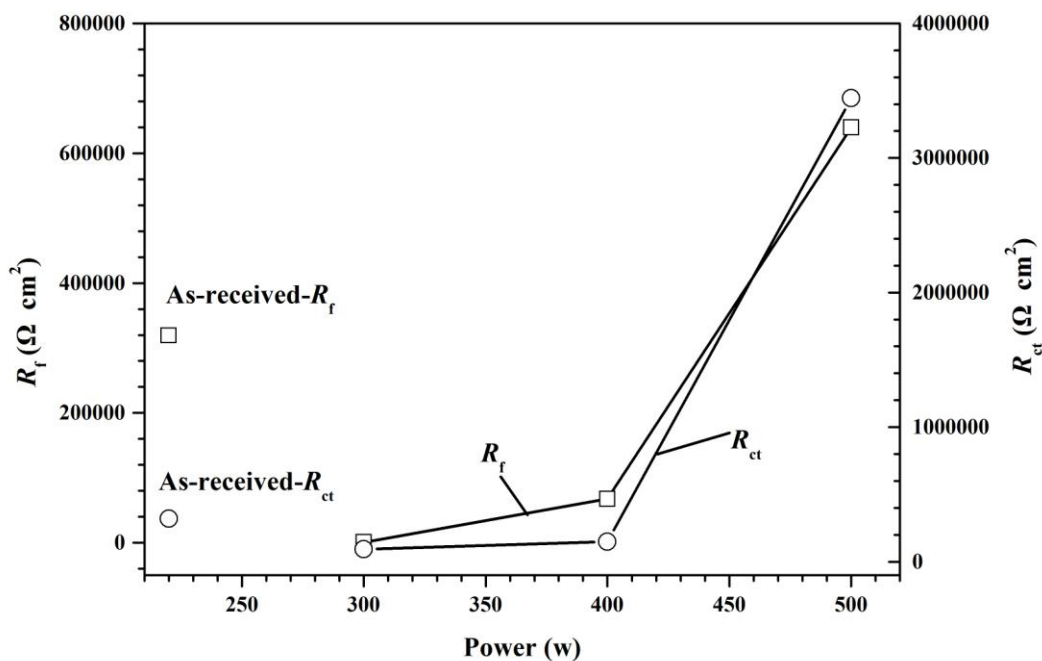
Figure 7. Fitted results of corrosion product film resistance R_f and charge transfer resistance R_{ct}
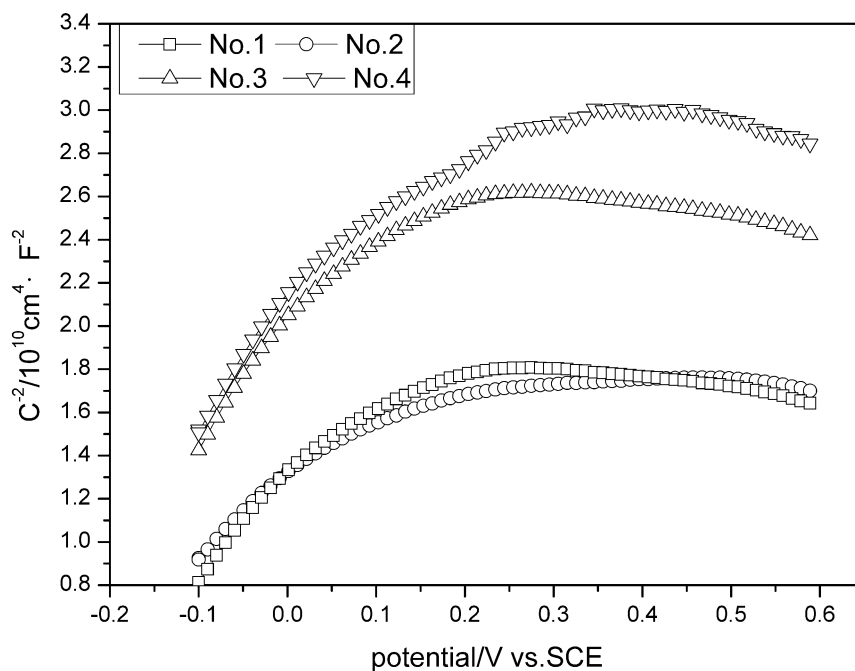

Figure 8. The Mott–Schottky plots of the samples.

The Mott–Schottky plots of the samples are shown in Fig. 8. The positive slopes obtained indicated that the passive films formed were n-type semiconductors. This result is different with the

passive films formed on stainless steel in H_2SO_4 solutions, which behave as dual n-type and p-type semiconductors. According to literature [19,20], passive films formed on stainless steel in H_2SO_4 solutions have bilayer structures, which have been generally assumed to consist of a Cr-rich inner layer with a p-type semiconducting behavior and a Fe-rich outer layer with an n-type semiconducting behavior. In the present study, based on the base metal and laser remelted samples, the passive behavior of austenitic stainless steel in artificial saliva has n-type semiconducting properties, which is different with that in H_2SO_4.

The donor density values (N_D) of the base metal and the samples subjected to 300, 400, and 500 W laser surface remelting were 3.2×10^{20}, 2.2×10^{20}, 3.4×10^{20}, and 3.6×10^{20} cm^{-3}, respectively, which were obtained from the Mott–Schottky plots. Notably, the N_D of sample No. 2 was lowest among the samples, which indicated that the ionic and electronic conductivities of the passive films on No. 2 sample were lowest among the samples. Nonetheless, the N_D values of No. 2 and No. 3 samples increased with increasing laser power.

The corrosion resistance of austenitic stainless steel depends on its phase composition and grain size. Generally, a small amount of δ second phase can improve corrosion resistance because it can disturb the direction of γ phase and avoid the continuous formation of poor Cr layer. Aleksandra Kocijana et. al. studied the evolution of the passive films on 2205 duplex stainless steel (2205 DSS) and AISI 316L stainless steel in artificial saliva, it is found that the corrosion characteristics of 2205 DSS are better than those of AISI 316L stainless steel. They attributed this to the effect of chemical composition on passive films [1]. However, the whole chemical composition of 316L in this study is keeping certain. The reason of changing of corrosion resistance maybe attributed to refined grain size. When the surface of austenitic stainless steel was remelted by laser, the recrystallization progress suppresses the precipitation of δ phase because of the rapid cooling property of laser remelting. However, refined grain sizes simultaneously improve the homogenization of surface elements, which increases the formation of the passive film. The homogenization of surface elements is attributed to rapid solidification, which inhibits the segregation of elements from a liquid metal. Given that the amount of δ phase decreased in the samples subjected to laser remelting, they should exhibit poor corrosion resistances. However, the refined grain sizes and the homogenization of surface elements offset the reduction of corrosion resistance. Therefore, the No. 2 sample demonstrated a better corrosion resistance than that of the base metal. By contrast, the grain sizes of No. 3 and No. 4 samples increased with increasing laser power, and they demonstrated worse corrosion resistances than that of the base metal. These results indicated that laser surface remelting can either improve or reduce the corrosion resistance of austenitic stainless steel depending on laser power. Only the appropriate laser power was found to improve the corrosion resistance of austenitic stainless steel. Moreover, high laser powers were unable to increase its corrosion resistance.

4. CONCLUSIONS

Laser surface remelting was used to improve the corrosion resistance of 316L orthodontic bracket in artificial saliva. The improvement of 316L orthodontic bracket was found to depend on the

laser power. Only the appropriate laser power was able to improve the corrosion resistance of 316L orthodontic bracket; higher laser powers were unable to increase its corrosion resistance. The passive films on 316L orthodontic bracket in artificial saliva were found to exhibit n-type semiconducting properties. The improved corrosion resistance of 316L orthodontic bracket was attributed to the refinement of its grain sizes and homogenization of its surface elements by laser remelting.

References

1. A. Kocijan, D.K. Merl and M. Jenko, *Corros. Sci.*, 53 (2011) 776.
2. A. Jose Ortiz, E. Fernandez, A. Vicente, J.L. Calvo and C. Ortiz, Am. J. Orthod. *Dentofacial Orthop.*, 140 (2011) E115.
3. A. Vahed, N. Lachman and R.D. Knutsen, *Dent. Mater.*, 23 (2007) 855.
4. C.H. Chen, K.L. Ou and W.N. Wang, *J. Exp. Clin. Med.*, 5 (2013) 30.
5. A. Kustarci and O. Sokucu, Photomed. *Laser Surg.*, 28 (2010) S57.
6. E. Ozyildiz, M. Guden, A. Uzel, I. Karaboz, O. Akil and H. Bulut, *Biotechnol. Bioprocess Eng.*, 15 (2010) 680.
7. D.C. Romonti, G. Voicu and M. Prodana, *Int. J. Electrochem. Sci.*, 10 (2015) 6935.
8. I. Milosev and H.H. Strehblow, *J. Biomed. Mater. Res.*, 52 (2000) 404.
9. A. Shahryari, S. Omanovic and J.A. Szpunar, *Mater. Sci. Eng.*, C, 28 (2008) 94.
10. C. Liu, G. Lin, D. Yang and M. Qi, *Surf. Coat. Technol.*, 200 (2006) 4011.
11. Y.W. Hao, B. Deng, C. Zhong, Y.M. Jiang, and J. Li, *Journal of Iron and Steel Research, International*, 16 (2009), 68.
12. J. Lv and T. Liang, Appl. *Surf. Sci.*, 359 (2015) 158.
13. X.S. Yuan, Y. Wang, L. Cao, B.C. Cao and J. Liang, *Corrosion*, 71 (2015) 784.
14. N. Mahato, M.R. Sharma, T.P. Chaturvedi and M.M. Singh, *Mater. Lett.*, 65 (2011) 2241.
15. M.J. Ziglo, A.E. Nelson, G. Heo and P.W. Major, *Appl. Surf. Sci.*, 255 (2009) 6790.
16. S.N. Dahotre, H.D. Vora, K. Pavani and R. Banerjee, *Appl. Surf. S*ci., 271 (2013) 141.
17. B. Du, A. N. Samant, S. R. Paital, and N. B. Dahotre, *Appl. Surf. Sci.*, 255 (2008), 3188.
18. W.C.Zhu, W. H. Leng, J. Q. Zhang, and C. N. Cao, *Acta Metallurgica Sinica (English Letters)*, 19 (2006), 91.
19. C.O.A. Olsson and D. Landolt, *Electrochim. Acta*, 48 (2003) 1093.
20. M.J. Carmezim, A.M. Simões, M.F. Montemor and M.D. Cunha Belo, *Corros. Sci.*, 47 (2005) 581.